MULTI-TASK LEARNING WITH LOW-RANK MATRIX FACTORIZATION FOR HYPERSPECTRAL NONLINEAR UNMIXING

Yuanchao Su[1], *Jun Li*[1], *Hairong Qi*[2], *Paolo Gamba*[3], *Antonio Plaza*[4] *and Javier Plaza*[4]

[1]Guangdong Provincial Key Laboratory of Urbanization and Geo-simulation,
School of Geography and Planning, Sun Yat-sen University, Guangzhou, 510275, China
[2]Department of Electrical Engineering and Computer Science,
University of Tennessee, Knoxville, TN 37996, USA
[3]Department of Electrical, Computer and Biomedical Engineering, University of Pavia, I-27100, Italy
[4]Department of Technology of Computers and Communications,
University of Extremadura, E-10003 Caceres, Spain

ABSTRACT

Nonlinear unmixing of hyperspectral images has been a very challenging research problem, as it needs to consider the physical interactions between the sunlight scattered by multiple materials. In this paper, we propose a new approach for nonlinear unmixing which is based on multi-task learning (MTL) with low-rank matrix factorization (LRMF). The proposed approach establishes two tasks to conduct the unmixing problem under a nonlinear mixing model. In the first task, we employ LRMF to obtain endmember signatures and their corresponding abundance fractions simultaneously. Then, the second task uses LRMF to solve interactions from multiple scattering. The effectiveness of the proposed method is verified by using real hyperspectral data. Compared with other state-of-the-art nonlinear unmixing algorithms, the proposed approach demonstrates very competitive performance.

Index Terms— Hyperspectral data, Nonlinear unmixing, Multi-Task Learning, Low-Rank Matrix Factorization

1. INTRODUCTION

Hyperspectral imaging has been extensively adopted in many fields [1, 2]. However, due to the relatively low spatial resolution of these images, several materials may be mixed in a pixel, which may lead to inaccuracies in the quantification of the considered scenes, thus limiting the application of hyperspectral data in a variety of applications [3, 4, 5]. The interpretation of mixed pixels mainly relies on spectral unmixing (SU) techniques [6, 7].

This work was supported by National Natural Science Foundation of China under Grant 61771496, National Key Research and Development Program of China under Grant 2017YFB0502900, Guangdong Provincial Natural Science Foundation under Grant 2016A030313254.

SU approaches are mainly based on two mixing models, including the linear spectral mixing model (LSMM) and the nonlinear spectral mixing model (NSMM) [8, 9]. LSMM is a simplified model which assumes that the photons reaching the sensor have interacted with just one material. Over the last few decades, most SU methods were developed under the LSMM considering its simplicity and efficiency. Nonetheless, it is known that the LSMM may not lead to a good approximation in many practical scenes. In contrast, NSMMs assume that the mixing should be nonlinear in real scenarios, due to physical interactions between the sunlight scattered by multiple materials [10]. To address the problem of multiple scattering, several works note that handling the second-order scattering is sufficient, while higher order terms can be neglected [11]. These mixing models are referred to as bilinear mixture models [11, 12]. Our proposed approach adopts the bilinear model to develop a new NSMM algorithm for hyperspectral images.

Multi-task learning (MTL) can perform multiple tasks in one step, which may improve the performance by exploiting shared representation across tasks [13, 14, 15]. Furthermore, MTL may help the final results avoid local minima through shared representation, because the local minima of different tasks are often in different positions [16]. Since SU may be regarded as the solution to an optimization problem, MTL may help to reduce the possibility that the results are trapped in local minima. Actually, MTL has been used to characterize multilinear models, which learn a bilinear mapping for modeling the interactions between tasks [13]. With respect to the bilinear model, the collinearity problem for endmembers and second-order scattering is a common phenomenon that may lead to a degradation of the performance of bilinear unmixing [17, 18]. Nonetheless, MTL may alleviate the effect of collinearity by adopting a shared representation of different tasks during the implementation of the unmixing process.

Low-rank matrix factorization (LRMF) is a widely used approach for extracting foreground and subtracting background from videos or images. Its main idea is to extract the low-rank approximation of the data matrix from the product of two smaller matrices, corresponding to the basis matrix and the coefficient matrix [19, 20]. With respect to the bilinear model, the SU formulation can be decomposed as two parts, including the linear part and the bilinear part. For the abundance estimation, considering the spatial information contained in the hyperspectral image, the linear part can be regarded as the objects of the foreground, while the interactions of the bilinear part resemble the camera jitters on the background.

In this work, we develop a new approach (named MLRMF) that combines MTL with LRMF for nonlinear unmixing of hyperspectral images. The proposed approach takes advantage of the aforementioned characteristics of MTL and LRMF to provide a completely new perspective on the nonlinear SU problem. The remainder of this paper is organized as follows. Section 2 introduces the proposed MLRMF approach. In section 3, we use the AVIRIS Moffett Field data to evaluate the proposed approach, conducting a quantitative comparison with other unmixing algorithms. Finally, section 4 concludes this work with some remarks.

2. PROPOSED APPROACH

The proposed MLRMF includes two main tasks. In the first task, which deals mainly with the linear part of the model, LRMF is employed to obtain a basis matrix and a coefficient matrix, corresponding to endmember signatures $\mathbf{E} \in \mathbb{R}^{d\times m}$ and abundance fractions $\mathbf{A} \in \mathbb{R}^{m\times n}$, respectively. In the second task, which deals with the bilinear part of the model, we also adopt LRMF to obtain two low-rank matrices, corresponding to a bilinear endmember matrix $\mathbf{D} \in \mathbb{R}^{d\times l}$ and an interacted abundance matrix $\mathbf{B} \in \mathbb{R}^{l\times n}$, respectively, where m denotes the number of endmembers, $l = m(m-1)/2$ denotes the number of bilinear components, n is the number of pixels, and d represents the number of bands [17]. Finally, the observed image $\mathbf{Y} \in \mathbb{R}^{d\times n}$ would be decomposed as the endmembers, abundances and the interactions of bilinear part. Following the assumptions in [12], the matrix form of the bilinear model is written as:

$$\begin{aligned} \mathbf{Y} = \ & \mathbf{EA} + \mathbf{DB} + \mathbf{N} \\ \text{s.t.: } & \mathbf{A} \geq 0, \mathbf{B} \geq 0, \mathbf{1}_m^T \mathbf{A} = \mathbf{1}_n^T, \end{aligned} \tag{1}$$

where $\mathbf{N}$ denotes the error matrix, e.g., Gaussian noise.

2.1. Objective function of MLRMF

By regularizing the error cost, the objective function is defined as follows:

$$\begin{aligned} (\mathbf{E}, \mathbf{A}, \mathbf{D}, \mathbf{B}) = \ & \arg\min \frac{1}{2}\|\mathbf{Y} - \mathbf{EA} - \mathbf{DB}\|_F^2 \\ & + f_1(\mathbf{E}, \mathbf{A}) + f_2(\mathbf{D}, \mathbf{B}), \end{aligned} \tag{2}$$

where $f_1(\mathbf{E}, \mathbf{A})$ and $f_2(\mathbf{D}, \mathbf{B})$ are the regularization terms for constraining the linear and bilinear parts, respectively.

In this work, we employ MTL to optimize the unmixing objective function. Following the SU basic formulation, the optimization problem is transformed to a regularized subproblem. In this paper, $\mathbf{E}$ and $\mathbf{A}$ are initialized by using vertex component analysis (VCA) [21] and fully constrained least squares (FCLS) [22], respectively. The bilinear matrix $\mathbf{D}$ and the corresponding coefficients $\mathbf{B}$ can then be initialized by $\mathbf{E}$ and $\mathbf{A}$. Following the bilinear model in [12, 17, 18], let $\forall\ i\ \in \{1, \ldots, m-1\}$, $j \in \{i+1, \ldots, m\}$, for the bilinear endmember $\mathbf{d}_{(i,j)}$, we have

$$\mathbf{d}_{(i,j)} = \mathbf{e}_i \odot \mathbf{e}_j, \tag{3}$$

where $\odot$ is the Hadamard product operation. With respect to $\mathbf{B}$, let $a_{i,q}$ and $a_{j,q}$ be the i-th element and the j-th element of the q-th column of $\mathbf{A}$, respectively, $b_{(i,j),q}$ be the element of the q-th column of $\mathbf{B}$, we have

$$b_{(i,j),q} = a_{i,q} a_{j,q}. \tag{4}$$

Finally, the reconstruction $\widehat{\mathbf{Y}}$ can be obtained as

$$\widehat{\mathbf{Y}} = \mathbf{EA} + \mathbf{DB}. \tag{5}$$

where the root-mean-square-error (RMSE) is given by

$$\text{RMSE}(\mathbf{Y}, \widehat{\mathbf{Y}}) = \frac{1}{2}\|\mathbf{Y} - \widehat{\mathbf{Y}}\|_F^2. \tag{6}$$

We emphasize that the training process stops when RMSE reaches a convergence threshold.

2.2. MLRMF for Task 1 (linear part of the SU model)

LRMF approximates the input matrix as the product of two small matrices [19]. For the first task, we assume that $\mathbf{A}$ and the transposition of $\mathbf{E}$ possess rational low-rank structures. Then, the objective function of the sub-problem is rewritten as:

$$\begin{aligned} (\mathbf{E}, \mathbf{A})_{\text{Task 1}} = \min_{\mathbf{E},\mathbf{A}} \|\mathbf{Y} - \mathbf{EA} - \mathbf{DB}\|_F^2 \ & + \mu_1 \Re_E(\mathbf{E}) \\ & + \upsilon_1 \|\mathbf{A}\|_*, \end{aligned} \tag{7}$$

where μ_1 and υ_1 are the coefficients of the sub-problem. The regularizations $\Re_E(\mathbf{E})$ and $\|\mathbf{A}\|_*$ are defined as:

$$\begin{cases} \Re_E(\mathbf{E}) = \sum_{i=1}^m (\mathbf{r}_i^T \mathbf{h}_i)^T \mathbf{r}_i^T \mathbf{h}_i, \\ \\ \|\mathbf{A}\|_* = \text{Tr}(\sqrt{\mathbf{A}^T \mathbf{A}}), \end{cases} \tag{8}$$

where $\mathrm{Tr}(\cdot)$ denotes the trace norm to impose low-rank, T represents matrix transposition,

$$\mathbf{r}_i = \mathbf{e}_i^t - \mathbf{e}_i^{t-1},$$

$$\mathbf{h}_i \leftarrow \vartheta\ \mathbf{r}_i\ \exp(-\frac{1}{2\sigma^2}\|\mathbf{r}_i\|_2^2), \tag{9}$$

where t denotes the number of iterations, we empirically set $\sigma = 4.5$ and $\vartheta = 0.9$, respectively.

With respect to $\mathbf{E}$ and $\mathbf{A}$, we employ the gradient descent for the solution,

$$\begin{aligned} \mathbf{E} &\leftarrow \mathbf{E} - \eta_E \nabla \mathbf{E}, \\ \mathbf{A} &\leftarrow \mathbf{A} - \eta_A \nabla \mathbf{A}. \end{aligned} \tag{10}$$

where $\nabla\mathbf{E}$ and $\nabla\mathbf{A}$ are gradients about $\mathbf{E}$ and $\mathbf{A}$, respectively. The corresponding learning rates η_E and η_A are estimated by Armijo rule [23].

2.3. MLRMF for Task 2 (bilinear part of the SU model)

In this work, the background possesses a low-rank structure, i.e., $\mathbf{B}$ is assumed to be a low-rank matrix. In the second task, the objective function is defined as follows:

$$(\mathbf{D}, \mathbf{B})_{\text{Task 2}} = \min_{\mathbf{D},\mathbf{B}} \|\mathbf{Y} - \mathbf{E}\mathbf{A} - \mathbf{D}\mathbf{B}\|_F^2 + \upsilon_2 \|\mathbf{B}\|_*, \tag{11}$$

where $\|\mathbf{B}\|_* = \mathrm{Tr}(\sqrt{\mathbf{B}^T\mathbf{B}})$, υ_2 is the regularization coefficient of the sub-problem. Since $\mathbf{B}$ is defined as a low-rank and non-negative structure, the solution can be obtained as follows

$$\mathbf{B} \leftarrow \mathrm{sgn}(\widetilde{\mathbf{B}}).*\max(\widetilde{\mathbf{B}} - \mathbf{\Lambda}_{\widetilde{B}}, 0), \tag{12}$$

where $\mathrm{sgn}(\cdot)$ is the sign function and $.*$ is the dot product, the threshold is given as $\mathbf{\Lambda}_{\widetilde{B}} = \lambda./(|\widetilde{\mathbf{B}}| + \lambda)$ with $\lambda = 0.001$ and

$$\widetilde{\mathbf{B}} = \mathbf{U}\ \mathrm{diag}(\widetilde{\mathbf{S}})\ \mathbf{V}^T,$$

where $\mathbf{U}, \mathbf{S}, \mathbf{V}$ are obtained by the singular value decomposition (SVD) of $\mathbf{B}$, i.e., $[\mathbf{U}, \mathbf{S}, \mathbf{V}] = \mathrm{SVD}(\mathbf{B})$ and $\widetilde{\mathbf{S}} = \max(|\mathrm{diag}(\mathbf{S})| - \mathbf{\Lambda}_S, 0)$, with $\mathbf{\Lambda}_S = \lambda./(|\mathrm{diag}(\mathbf{S})| + \lambda)$.

Finally, we update the bilinear endmember matrix $\mathbf{D}$ as follows:

$$\mathbf{D} \leftarrow \mathbf{D}. * (\mathbf{Y} - \mathbf{E}\mathbf{A})\mathbf{B}^T./\mathbf{D}\mathbf{B}\mathbf{B}^T. \tag{13}$$

3. EXPERIMENTAL RESULTS

The effectiveness of the proposed MLRMF is evaluated by using a real hyperspectral image, which was acquired over Moffett Field, CA, USA in 1997 by the Airborne Visible Infra-Red Imaging Spectrometer (AVIRIS) [24]. In this paper, we use a sub-image of 50×50 pixels. It includes 189 bands covering the wavelengths from 0.4μm to 2.5μm and is comprised of vegetation, soil, and water. Noted that the low signal-to-noise ratio (SNR) and the water-absorption bands were removed from the sub-image.

Table 1. Reconstruction errors ($\times 10^{-2}$) obtained by different unmixing methods for the AVIRIS Moffett Field image.

Method	VCA+FCLS	VCA+GBM	VCA+Semi-NMF
RE	2.0843	2.0131	1.9905
Method	rNMF	MLRMF	
RE	1.9610	1.9463	

Here, we evaluate the proposed MLRMF by comparing with several classical unmixing algorithms, such as FCLS [22], generalized bilinear model (GBM) [11], Semi-Nonnegative Matrix Factorization (Semi-NMF) [17], and robust nonnegative matrix factorization (rNMF) [25]. It should be noted that FCLS is a linear unmixing method, while the rest are nonlinear unmixing approaches. Moreover, FCLS, GBM, and Semi-NMF only obtain abundance fractions, while rNMF and the proposed MLRMF can estimate both endmembers and abundances. In this paper, we use VCA to extract endmembers signatures before running FCLS, GBM, and Semi-NMF. Due to lack of library signatures, we just use reconstruction error (RE) to assess the accuracy of the unmixing results, which is given as follows:

$$\mathrm{RE}(\{\mathbf{y}_q\}_{q=1}^n, \{\overline{\mathbf{y}}_q\}_{q=1}^n) = \tfrac{1}{n}\textstyle\sum_{q=1}^n \sqrt{\|\mathbf{y}_q - \overline{\mathbf{y}}_q\|_2^2}, . \tag{14}$$

where $\overline{\mathbf{Y}} = \mathbf{E}\mathbf{A} \in \mathbb{R}^{d\times n}$ is the data reconstructed by $\mathbf{E}$ and $\mathbf{A}$ [26, 27, 28]. The quantitative results are shown in Table 1. It can be observed that the proposed MLRMF obtained the best result.

For illustrative purposes, Fig.1 shows the abundance maps, estimated endmembers, and bilinear interactions on abundances. These visual maps further demonstrate the effectiveness of the proposed MLRMF for hyperspectral unmixing purposes.

4. CONCLUSIONS

This paper introduced a new approach for nonlinear unmixing, which includes two main parts: 1) linear unmixing of the foreground and 2) bilinear unmixing of the background. The approach is based on the assumption that, in order to address the multiple scattering problem, handling the second-order scattering is sufficient, while higher order terms can be neglected. The proposed method combines multi-task learning (MTL) with low-rank matrix factorization (LRMF) to perform accurate nonlinear unmixing of hyperspectral scenes. Our newly developed MLRMF method is able to obtain endmember signatures, abundance fractions, and the

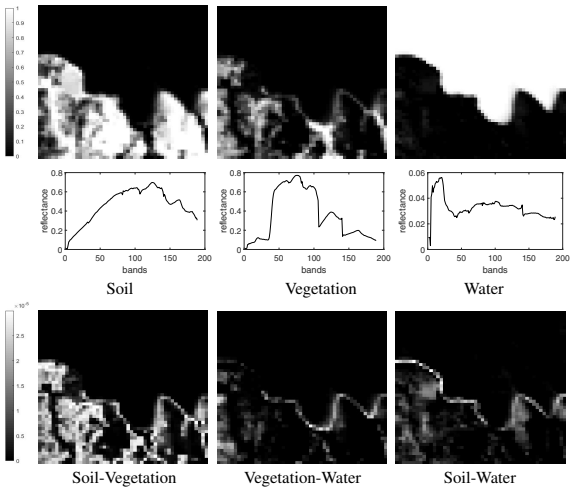

Fig. 1. The results obtained by the proposed MLRMF on the Moffett dataset. Top: abundance maps (matrix **A**). Middle: estimated endmember signatures (matrix **E**). Bottom: bilinear interactions on abundances (matrix **B**).

bilinear interactions on endmembers and abundances, in one step. By taking advantage of MTL, the collinearity and local convergence problems are alleviated. Our experimental results showed that the proposed approach provides competitive performance when compared to other nonlinear unmixing approaches. Future work will be focused on conducting a more exhaustive evaluation of the proposed approach using additional hyperspectral scenes and both linear/nonlinear unmixing methods.

5. REFERENCES

[1] J. M. Bioucas-Dias, A. Plaza, N. Dobigeon, M. Parente, Q. Du, P. Gader, and J. Chanussot, "Hyperspectral unmixing overview: Geometrical, statistical, and sparse regression-based approaches," *IEEE J., Sel. Topics Appl. Earth Observ. and Remote Sens.*, vol. 5, no. 2, pp. 354–379, Apr. 2012.

[2] L. Zhang, W. Wei, Y. Zhang, C. Shen, A. Hengel, and Q. Shi, "Cluster sparsity field: An internal hyperspectral imagery prior for reconstruction," *International Journal of Computer Vision*, vol. 126, no. 8, pp. 797–821, Aug. 2018.

[3] Y. Gu, J. Chanussot, X. Jia, and J. A. Benediktsson, "Multiple kernel learning for hyperspectral image classification: A review," *IEEE Trans. Geosci. and Remote Sens.*, vol. 55, no. 11, pp. 6547–6565, Nov. 2017.

[4] X. Jin and Y. Gu, "Superpixel-based intrinsic image decomposition of hyperspectral images," *IEEE Trans. Geosci. and Remote Sens.*, vol. 55, no. 8, pp. 4285–4295, Aug. 2017.

[5] L. Zhang, W. Wei, C. Bai, Y. Gao, and Y. Zhang, "Exploiting clustering manifold structure for hyperspectral imagery super-resolution," *IEEE Trans. Image Process.*, vol. 27, no. 12, pp. 5969–5982, Dec. 2018.

[6] D. Manolakis, C. Siracusa, and G. Shaw, "Hyperspectral subpixel target detection using the linear mixing model," *IEEE Trans. Geosci. and Remote Sens.*, vol. 39, no. 7, pp. 1392–1409, 2001. Jul.

[7] Y. Su, X. Sun, L. Gao, J. Li, and B. Zhang, "Improved discrete swarm intelligence algorithms for endmember extraction from hyperspectral remote sensing images," *J. Appl. Rem. Sens.*, vol. 10, no. 4, pp. 1–19, Nov. 2016.

[8] R. Heylen, M. Parente, and P. Gader, "A review of nonlinear hyperspectral unmixing methods," *IEEE J., Sel. Topics Appl. Earth Observ. and Remote Sens.*, vol. 7, no. 6, pp. 1844–1868, Jun. 2014.

[9] M. Tang, L. Gao, A. Marinoni, P. Gamba, and B. Zhang, "Integrating spatial information in the normalized p-linear algorithm for nonlinear hyperspectral unmixing," *IEEE J., Sel. Topics Appl. Earth Observ. and Remote Sens.*, vol. 11, no. 4, pp. 1179–1190, Apr. 2018.

[10] N. Dobigeon, J. Y. Tourneret, C. Richard, J. C. M. Bermudez, S. McLaughlin, and A. O. Hero, "Nonlinear unmixing of hyperspectral images: Models and algorithms," *IEEE Signal Processing Mag.*, vol. 31, no. 1, pp. 82–94, Jan. 2014.

[11] A. Halimi, Y. Altmann, N. Dobigeon, and J. Tourneret, "Nonlinear unmixing of hyperspectral images using a generalized bilinear model," *IEEE Trans. Geosci. and Remote Sens.*, vol. 49, no. 11, pp. 4153–4162, Nov. 2011.

[12] W. Fan, B. Hu, J. Miller, and M. Li, "Comparative study between a new nonlinear model and common linear model for analysing laboratory simulated-forest hyperspectral data," *Int. J. Remote Sens.*, vol. 30, no. 11, pp. 2951–2962, Jun. 2009.

[13] C.-T. Lu, L. He, W. Shao, B. Cao, and P. S. Yu, "Multilinear factorization machines for multi-task multi-view learning," *Proceedings of the Tenth ACM International Conference on Web Search and Data Mining*, vol. 9, no. 2, pp. 354–379, Apr. 2012.

[14] C. Li, Z. Wang, and H. Qi, "Fast-converging conditional generative adversarial networks for image synthesis," *2018 25th IEEE International Conference on Image Processing (ICIP)*, pp. 2132–2136, Oct. 2018.

[15] G. Gao and Y. Gu, "Tensorized principal component alignment: A unified framework for multimodal high-resolution images classification," *IEEE Trans. Geosci. and Remote Sens.*, vol. 57, no. 1, pp. 46–61, Jan. 2019.

[16] A. Argyriou, T. Evgeniou, and M. Pontil, "Convex multi-task feature learning," *Machine Learning*, vol. 73, no. 3, pp. 243–272, Dec. 2008.

[17] N. Yokoya, J. Chanussot, and A. Iwasaki, "Nonlinear unmixing of hyperspectral data using semi-nonnegative matrix factorization," *IEEE Trans. Geosci. and Remote Sens.*, vol. 52, no. 2, pp. 1430–1437, Feb. 2014.

[18] B. Yang, B. Wang, and Z. Wu, "Nonlinear hyperspectral unmixing based on geometric characteristics of bilinear mixture models," *IEEE Trans. Geosci. and Remote Sens.*, vol. 56, no. 2, pp. 694–714, Feb. 2018.

[19] H. Yong, D. Meng, W. Zuo, and L. Zhang, "Robust online matrix factorization for dynamic background subtraction," *IEEE Trans.Pattern Anal. Mach. Intell.*, vol. 40, no. 7, pp. 1726–1740, Jul. 2018.

[20] W. Wei, L. Zhang, Y. Jiao, C. Tian, C. Wang, and Y. Zhang, "Intracluster structured low-rank matrix analysis method for hyperspectral denoising," *IEEE Trans. Geosci. and Remote Sens.*, vol. PP, no. 99, pp. 1–15, Aug. 2018.

[21] J. M. P. Nascimento and J. M. Dias-Bioucas, "Vertex component analysis: A fast algorithm to unmix hyperspectral data," *IEEE Trans. Geosci. and Remote Sens.*, vol. 43, no. 4, pp. 898–910, Apr. 2005.

[22] D. C. Heinz and C.-I Chang, "Fully constrained least squares linear spectral mixture analysis method for material quantification in hyperspectral imagery," *IEEE Trans. Geosci. and Remote Sens.*, vol. 39, no. 3, pp. 529–545, Mar.2001.

[23] J. Nocedal and S. J. Wright, "Numerical optimization," *New York, NY, Springer*, pp. 33–36, 2006.

[24] E. Christophe, D. Leger, and C. Mailhes, "Quality criteria benchmark for hyperspectral imagery," *IEEE Trans. Geosci. and Remote Sens.*, vol. 43, no. 9, pp. 2103–2114, Sep. 2005.

[25] C. Fevotte and N. Dobigeon, "Nonlinear hyperspectral unmixing with robust nonnegative matrix factorization," *IEEE Trans. Image Process.*, vol. 24, no. 12, pp. 4810–4819, Dec. 2015.

[26] Y. Su, A. Marinoni, J. Li, J. Plaza, and P. Gamba, "Stacked nonnegative sparse autoencoders for robust hyperspectral unmixing," *IEEE Geosci Remote Sens. Lett.*, vol. 15, no. 9, pp. 1427–1431, Sep. 2018.

[27] Y. Su, J. Li, A. Plaza, A. Marinoni, P. Gamba, and S. Chakravortty, "Daen: Deep auto-encoder networks for hyperspectral unmixing," *IEEE Transactions on Geoscience and Remote Sensing*, vol. pp, no. Early Access, pp. 1–13, Dec. 2018.

[28] M. Tang, B. Zhang, A. Marinoni, L. Gao, and P. Gamba, "Multiharmonic postnonlinear mixing model for hyperspectral nonlinear unmixing," *IEEE Geosci Remote Sens. Lett.*, vol. 15, no. 11, pp. 1765–1769, Nov. 2018.